Proceedings of the 14th International Heat Transfer Conference
IHTC14
August 8-13, 2010, Washington, DC, USA

IHTC14-22439

FLOW CHARACTERISTICS AND STRUCTURES OF THREE-DIMENSIONAL UNSTEADY THERMAL CONVECTION IN A CONTAINER

Satoshi Fujita
Department of Mechanical Engineering
Doshisha University
Kyoto 610-0321, Japan

Hirochika Tanigawa
Department of Mechanical Engineering
Maizuru National College of Technology
Maizuru 625-8511, Japan

Jiro Funaki
Department of Mechanical Engineering
Doshisha University
Kyoto 610-0321, Japan

Katsuya Hirata
Department of Mechanical Engineering
Doshisha University
Kyoto 610-0321, Japan

ABSTRACT

In this study, we numerically investigates the flow and thermal characteristics of the three-dimensional thermal convection in a cubic cavity heated below in the gravitational field, concerning about spatially-averaged kinetic energy $\overline{K}$, Nusselt number Nu and flow structure. We assume Prandtl number Pr = 7.1 (water) and Rayleigh number $Ra = 1.0\times10^4$ — 3.5×10^5. As a result, we have specified two of three important values of the Rayleigh number which demarcate different flow bifurcations and are referred to as the second and third critical Rayleigh numbers Ra_{c2} and Ra_{c3}. We have found that Ra_{c2} and Ra_{c3} are roughly 2.6×10^5 and 3.1×10^5, respectively. We have observed a histerisis effect upon the value of Ra_{c2} with chaotic behaviour at $Ra \approx Ra_{c2}$, and revealed flow structures. In addition, we investigate the relationship between Ra and the oscillatory-convection frequency. The increasing rate of the $\overline{K}_{mean}$ with increasing Ra shows a different manner from that of $Nu_{inflow\text{-}ave,\ mean}$. That is, the former is progressive and the latter is asymptotic, as Ra increases. Both the values of $\overline{K}_{mean}$ and $Nu_{inflow\text{-}ave,\ mean}$ in oscillatory flow tend to be smaller than those in steady flow, respectively. Then, there exist small jumps/drops of $\overline{K}_{mean}$ and $Nu_{inflow\text{-}ave,\ mean}$ at $Ra = Ra_{c2}$.

INTRODUCTION

Thermal convection has been a key phenomenon for heat and mass transfers. So, a lot of researches have studied about the thermal convection. Also, the thermal convection is treated in such various fields as geology, meteorology, safety aspect of atomic reactor and manufacturing industries, and becomes important for mass and heat transfers/diffusions and material mixings in many appliances.

In the present study, we consider the three-dimensional thermal convection in one of the most fundamental and simplest containers; that is, a cubic cavity heated below in the gravitational field.

A lot of researchers have studied the cubic cavity. For example, Janssen et al.(1) numerically studied bifurcations from steady flow to periodical flow in a cubic cavity. Pallares et al. showed numerically the three-dimensional convection in a cubic cavity at moderate Rayleigh numbers Ra's < 6.0×10^4(2), (3), and showed experimentally and numerically it at high Ra's < 10^8(4), (5). They reported seven different steady-flow structures; namely, four kinds of single-roll structures (S1, S2, S3 and S7), two kinds of four-roll structures (S5 and S6), and one kind of a toroidal-roll structure (S4) (3). We should note that there are three important values of Ra which demarcate different flow bifurcations. There are referred to as the first, second and third critical Rayleigh numbers Ra_{c1}, Ra_{c2} and Ra_{c3}. Ra_{c1}, Ra_{c2} and Ra_{c3} indicate the transitions to steady flow, oscillatory flow and turbulent flow, respectively. Hirano et al.(6) and Brown et al.(7) conducted experiments at $Ra = 10^4$ — 10^5 and 10^8 — 10^{12}, respectively. Crunkleton et al.(8) specified the value of Ra_{c2} for a low Prandlt number Pr = 0.008, concerning cavities including a cubic one. Recently, Hirata et al.(9), Bennet & Hsueh(10) and Valencia et al.(11) have numerically shown detailed flow structures at middle and high Ra's.

Now, we have the knowledge about thermal convection in the wide range of Ra. However, the chaotic transition process from the laminar to turbulent flows has not been clear yet, due to its complexity. So, we numerically investigates the details of the flow and thermal characteristics of the three-dimensional thermal convection in a cubic cavity at the transition rage of Ra. Especially, we consider spatially-averaged kinetic energy $\bar{K}$, Nusselt number Nu and flow structure. Here, we assume incompressible fluid with Pr = 7.1 (water) and Ra = 1.0×10^4 — 3.5×10^5. Both bottom and top walls are taken to be isothermal, and the bottom temperature is greater than the top temperature. Four vertical walls are conductive. We try to determine the value of Ra_{c2} and Ra_{c3}. In addition, we investigate the relationship between the Rayleigh number and the oscillatory frequency of the convective flow at $Ra > Ra_{c2}$.

METHOD

We analyse the convection assuming incompressible fluid with a constant Prandtl number Pr = 7.1 (water) in the gravitational field. Tested Rayleigh number Ra is fixed to 1.0×10^4 — 3.5×10^5. Both bottom and top walls are taken to be isothermal, and the bottom temperature is greater than the top one. Four vertical sidewalls are conductive. Under these conditions, the flow attains a steady state or oscillatory state with such a flow structure as the S1, S2, S5, S6 or $S5_p$ after enough time (see later) or attains a chaotic or turbulent state referred to as Chaotic.

Governing Equation

The dimensionless Navier-Stokes equations with the Boussinesq approximation and an energy equation are as follows;

$$\nabla \cdot \boldsymbol{u} = 0, \tag{1}$$

$$\frac{\mathrm{D}\boldsymbol{u}}{\mathrm{D}t} = -\nabla p + Pr\,\Delta\boldsymbol{u} + Ra\,Pr\,T\boldsymbol{e}_z, \tag{2}$$

and

$$\frac{\mathrm{D}T}{\mathrm{D}t} = \Delta T. \tag{3}$$

where $\boldsymbol{u}$, t, p, T, $\boldsymbol{e}_z$ and ω denote velocity vector, time, pressure, temperature, the unit vector in the z direction and (angular) frequency, respectively.

Independent variables are non-dimensionalised as follows;

$$x = \begin{pmatrix} x \\ y \\ z \end{pmatrix} = \frac{1}{H^*}\begin{pmatrix} x^* \\ y^* \\ z^* \end{pmatrix}, \text{ and } t = \frac{t^*}{H^{*2}/\alpha^*}. \tag{4}$$

As well, dependent variables are non-dimensionalised as follows;

$$\boldsymbol{u} = \begin{pmatrix} u \\ v \\ w \end{pmatrix} = \frac{H^*}{\alpha^*}\begin{pmatrix} u^* \\ v^* \\ w^* \end{pmatrix}, \quad T = \frac{T^* - T_c^*}{T_h^* - T_c^*}, \text{ and } p = \frac{p^* H^{*2}}{\rho^* \alpha^{*2}}, \tag{5}$$

where α^*, T_c^*, T_h^*, and ρ^* denote the coefficient of thermal diffusivity, a cold top-wall temperature, a hot bottom-wall temperature and mean density, respectively. A superscript "*" represents to be dimensional.

Governing Parameter

Non-dimensional governing parameters are as follows.

$$\text{Rayleigh number:} \quad Ra = \frac{g^* \beta^* \left(T_h^* - T_c^*\right)}{\upsilon^* \alpha^*}. \tag{6}$$

And,

$$\text{Prandtl number:} \quad Pr = \frac{\upsilon^*}{\alpha^*}. \tag{7}$$

Here, β^*, υ^*, and g^* denote thermal expansion coefficient, kinetic viscosity, and the gravitational acceleration, respectively.

Boundary Condition

Boundary conditions for velocity are as follows.

$$u = v = w = 0 \qquad \text{(on all walls)} \tag{8}$$

Boundary conditions for pressure are given by the Navier-Stokes equations (2) with the no-slip condition of equation (8). Boundary conditions for temperature are as follows.

$$T = 1, \qquad \text{(at z = 0)} \tag{9}$$

$$T = 0, \qquad \text{(at z = 1)} \tag{10}$$

and

$$\frac{\partial T}{\partial z} = -1. \qquad (\text{at } x = 0,\ x = 1,\ y = 0 \text{ and } y = 1) \tag{11}$$

In equation (11), we consider thermally conductive conditions on four sidewalls.

Numerical Method

The governing equations (1) — (3) are solved by a finite difference method based on the MAC scheme with a staggered computational grid with a size of 81^3. The present flow is calculated at a time step Δt = 5.0×10^{-7}. Figure 1 shows the computational domain to be analysed, together with the present coordinate system and boundary conditions.

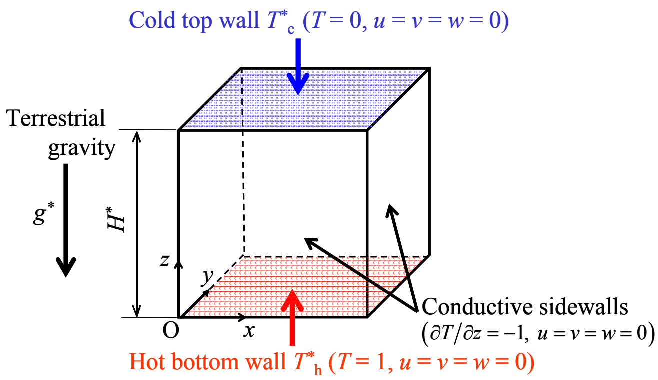

Fig. 1 Computational domain, together with coordinate system and boundary conditions.

Table 1 Accuracy check: a comparison on the Nusselt number averaged over a heated bottom-wall surface between Pallares et al. [(2), (3)] and the present study with an adiabatic-sidewall boundary condition.

Ra	Pr	Flow structure	$Nu_{\text{inflow-ave}}$ Pallares et al.	$Nu_{\text{inflow-ave}}$ Present	Error (%)
8.0×10^3	0.71	S2	1.70[(3)]	1.77	4.12
8.0×10^3	1	S1	1.755[(2)]	1.79	1.99
6.0×10^4	0.71	S1	3.13[(3)]	3.19	1.92

Global Indicators

As global indicators, we consider such physical quantities as a spatially-averaged kinetic energy $\overline{K}$ and an inflow-average Nusselt number $Nu_{\text{inflow-ave}}$. These are defined as follows.

$$\overline{K} = \frac{1}{V}\iiint_V K dV \ . \tag{15}$$

Here, K denotes the kinetic energy defined as

$$K = \frac{1}{2}\left(u^2 + v^2 + w^2\right),$$

and V denotes the volume of the cavity.

$$Nu_{\text{inflow-ave}} = \frac{\iint_{A_{\text{inflow}}} Nu_{\text{local}}\, dA}{H^2} \ . \tag{16}$$

Here, Nu_{local} denotes a local Nusselt number, and A_{inflow} denotes the total area of the bottom-wall surface and the sidewall surfaces where Nu_{local} is positive. Because the four sidewalls are conductive, some parts of the sidewalls can allow the inflow of heat as well as the bottom wall. Then, $Nu_{\text{inflow-ave}}$ represents the total inflow of heat normalised by an area H^2. We should note that both $\overline{K}$ and $Nu_{\text{inflow-ave}}$ are functions of time t.

RESULTS AND DISCUSSION

Numerical Accuracy

In order to confirm the present numerical accuracy, we investigate the flow with an adiabatic-sidewall boundary condition for $Ra = 8.0\times10^3$ and for $Pr = 0.71$ and 1, in some preliminary computations. These are the same conditions as Pallares et al.[(2), (3)] Table 1 shows a result for the accuracy check: a comparison on the Nusselt number averaged over a heated bottom-wall surface between Pallares et al.[(2), (3)] and the present study. We can confirm a good agreement between them.

Flow Structures

As shown in Fig. 2, we reveal the flow structures for $Pr = 7.1$ as a function of Ra. The results for $Ra \leq 8.0\times10^4$ are by Hirata et al.[(9)] The upper row in the figure corresponds to decreasing Ra, and the lower row corresponds to increasing Ra. Specifically speaking, the upper row indicates the flow structure solved using the solution at a higher Ra as an initial condition, and the lower row is *vi-ce versa*.

In Fig. 2, we can observe four kinds of steady flow structures; namely, two single-roll structures and two four-roll structures (as will be shown latter). These steady flow structures are referred to as S1, S2, S5 and S6, respectively, by Pallares et al.[(3), (4)] In addition to these four steady flow structures, we can observe two kinds of unsteady flow structures, which are referred to as $S5_p$ and Chaotic. The $S5_p$ is a periodic flow structure with the S5 at each instance. The Chaotic is not periodic (as will be shown latter).

From the figure, we can specify two of three important values of the Ra which demarcate different flow bifurcations — Ra_{c2} and Ra_{c3}, indicating the transition to oscillatory flow and the transition to chaotic or turbulent flow, respectivery. We can find that Ra_{c2} and Ra_{c3} are roughly 2.6×10^5 and 3.1×10^5 respectively. In addition, we can observe a histerisis effect upon the value of Ra_{c2}, with chaotic behaviour at $Ra \simeq Ra_{c2}$. Incidentally, Ra_{c1} is 8.0×10^3, which indicates the transition to conduction and steady flow.

Figures 3, 4, 5 and 6 show the typical flow structures for the S2, S1, S5 and S6, respectively. In each figure, figure (a) represents a perspective view of velocity vectors on the three horizontal plane at z = 0.25, 0.5 and 0.75, where each arrow's colour denotes the value of w as shown in a colour bar on its left side. As well, figure (b) represents top view of velocity vectors on the horizontal plane at z = 0.5. Figure (c) represents velocity vectors on a vertical diagonal section, where each arrow's colour denotes the value of T as shown in a colour bar on its left side. As well, figure (d) represents velocity vectors on the other vertical diagonal section.

The S2 is featured by the single roll with a horizontal axis on a vertical diagonal-section plane. On the other hand, the S1 is featured by the single roll with a horizontal axis on a vertical mid-plane, which are perpendicular to a pair of opposite sidewalls. For both the S2 and the S1, we can clearly recognise a single-roll structure.

The S5 is featured as both a pair of upward centripetal flows on a vertical diagonal-section plane and a pair of downward centripetal flows on the other vertical diagonal-section plane. On the other hand, the S6 is featured as both a pair of upward centripetal flows on a vertical mid-plane and a pair of downward centripetal flows on the other vertical diagonal-section plane.

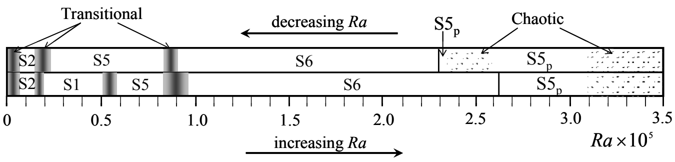

Fig. 2 Flow structures for $Ra \leq 3.5\times10^5$ and $Pr = 7.1$.

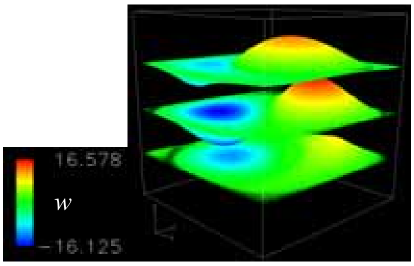

(a) Perspective view of velocity vectors on the three horizontal plane at z = 0.25, 0.5 and 0.75. Each arrow's colour denotes the value of w as shown in a colour bar.

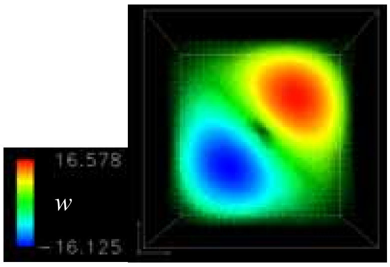

(b) Top view of velocity vectors on the horizontal plane at z = 0.5. Each arrow's colour denotes the value of w as shown in a colour bar.

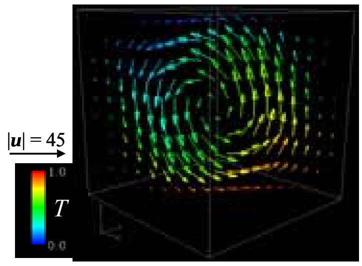

(c) Velocity vectors on a vertical diagonal section. Each arrow's colour denotes the value of T as shown in a colour bar.

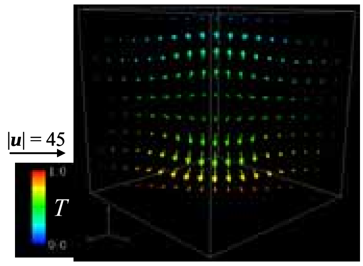

(d) Velocity vectors on the other vertical diagonal section. Each arrow's colour denotes the value of T as shown in a colour bar.

Fig. 3 Flow structure S2, for *Ra* = 1.0 × 10^4 and *Pr* = 7.1 with increasing *Ra*.

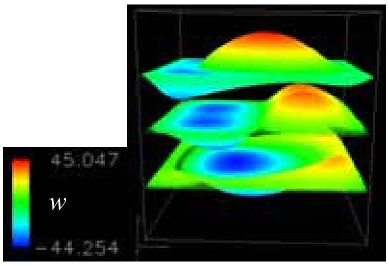

(a) Perspective view of velocity vectors on the three horizontal plane at z = 0.25, 0.5 and 0.75. Each arrow's colour denotes the value of w as shown in a colour bar.

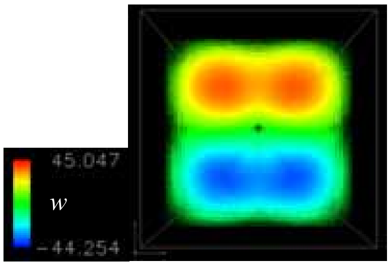

(b) Top view of velocity vectors on the horizontal plane at z = 0.5. Each arrow's colour denotes the value of w as shown in a colour bar.

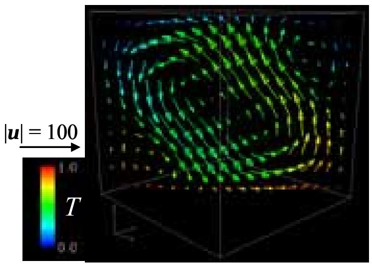

(c) Velocity vectors on a vertical diagonal section. Each arrow's colour denotes the value of T as shown in a colour bar.

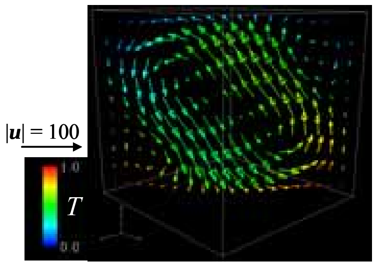

(d) Velocity vectors on the other vertical diagonal section. Each arrow's colour denotes the value of T as shown in a colour bar.

Fig. 4 Flow structure S1, for *Ra* = 4.0 × 10^4 and *Pr* = 7.1 with increasing *Ra*.

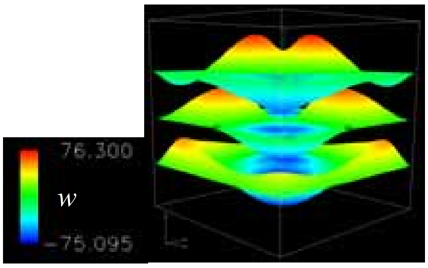

(a) Perspective view of velocity vectors on the three horizontal plane at z = 0.25, 0.5 and 0.75. Each arrow's colour denotes the value of w as shown in a colour bar.

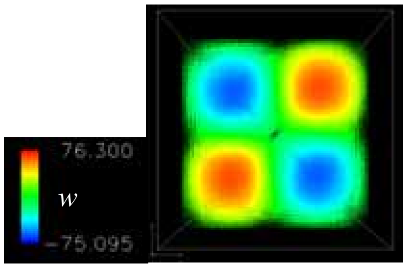

(b) Top view of velocity vectors on the horizontal plane at z = 0.5. Each arrow's colour denotes the value of w as shown in a colour bar.

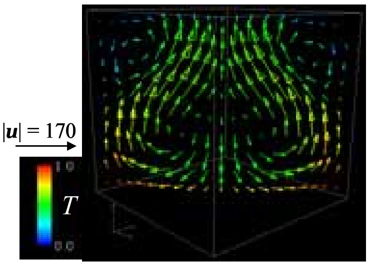

(c) Velocity vectors on a vertical diagonal section. Each arrow's colour denotes the value of T as shown in a colour bar.

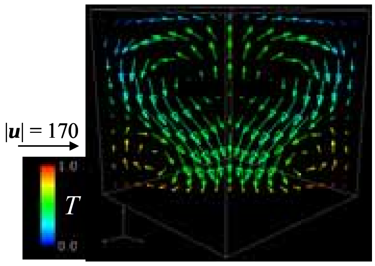

(d) Velocity vectors on the other vertical diagonal section. Each arrow's colour denotes the value of T as shown in a colour bar.

Fig. 5 Flow structure S5, for *Ra* = 8.0 × 10^4 and *Pr* = 7.1 with increasing *Ra*.

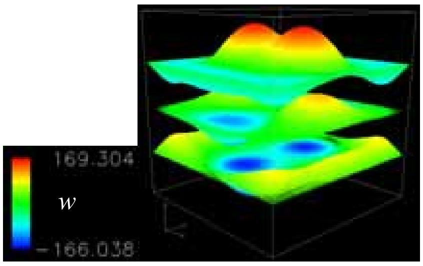

(a) Perspective view of velocity vectors on the three horizontal plane at z = 0.25, 0.5 and 0.75. Each arrow's colour denotes the value of w as shown in a colour bar.

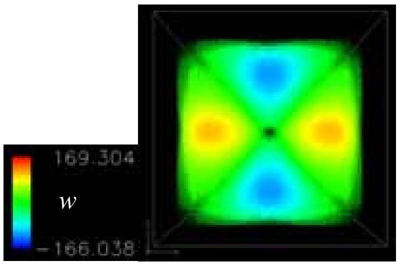

(b) Top view of velocity vectors on the horizontal plane at z = 0.5. Each arrow's colour denotes the value of w as shown in a colour bar.

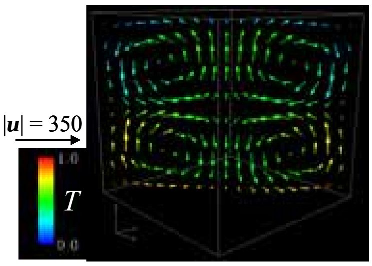

(c) Velocity vectors on a vertical diagonal section. Each arrow's colour denotes the value of T as shown in a colour bar.

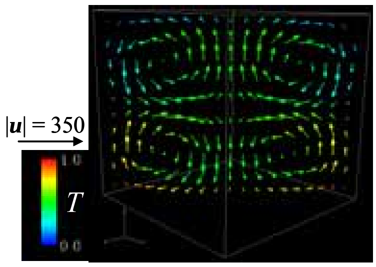

(d) Velocity vectors on the other vertical diagonal section. Each arrow's colour denotes the value of T as shown in a colour bar.

Fig. 6 Flow structure S6, for *Ra* = 18.0 × 10^4 and *Pr* = 7.1 with increasing *Ra*.

According to Paraller et al.[4] both the S5 and S6 are defined as four-roll structures. However, it seems difficult to find out such four-roll structures in Figs. 5 and 6. Figure 7 shows a stream line together with an iso-kinetic surface of $0.2\times\overline{K}_{\max}$, for $Ra = 8.0\times10^4$ and $Pr = 7.1$, in order to visualise a typical S5. When we see the iso-kinetic surface, it seems difficult to find out the four-roll structure as well as Fig. 5. The four-roll structure can be clearly visualised by streamlines with low velocity magnitudes near the sidewalls (see Fig.4 in Paraller et al.[3]). The streamline in Fig. 7, which has high velocity magnitudes, is considered to represent one of the distorted rolls of the four-roll structure.

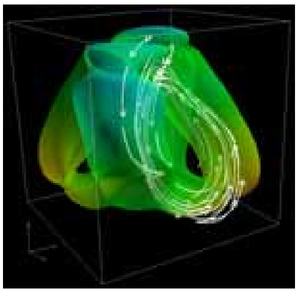

Fig. 7 One of the four rolls in S5 visualised by a stream line for $Ra = 8.0 \times 10^4$ and $Pr = 7.1$, with an iso-kinetic-surface of $0.2 \times K_{\max}$.

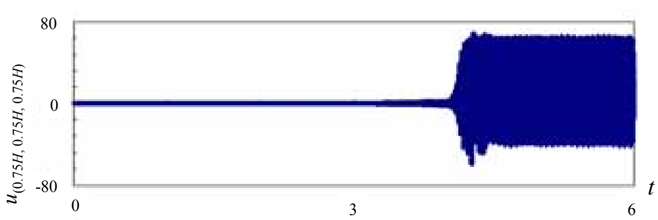

(a) Overall view (at $t = 0 – 6.0$)

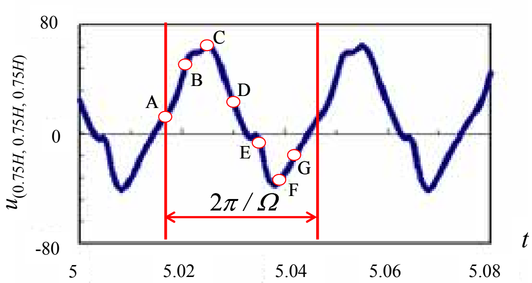

(b) Close-up view (at $t = 5.0 – 5.0894$)

Fig. 8 Time history of $u_{(0.75H,\,0.75H,\,0.75H)}$, for $Ra = 2.65 \times 10^5$ and $Pr = 7.1$ with increasing Ra ($S5_p$).

Frequency of $S5_p$ and Chaotic

Figure 8 shows a time history of $u_{(0.75H,\,0.75H,\,0.75H)}$ for $Ra = 2.65\times10^5$ and $Pr = 7.1$ with increasing Ra, which corresponds to the $S5_p$. Figures (a) and (b) are overall and close-up views, respectively.

We can confirm an exact periodicity with a dominant frequency Ω, long time after the beginnings of computations. However, its wave form is far from sinusoidal (see figure (b)).

Supplementary speaking, the points A — G in Fig. 8(b) denote the instants chosen for the flow visualisations in Fig. 9. Now, we consider the flow structure of the $S5_p$. Figure 9 shows the consecutive series of flow structures during one period $2\pi/\Omega$, for $Ra = 2.65\times10^5$ and $Pr = 7.1$ with increasing Ra. Namely, at each instant, we show a perspective view of velocity vectors on the three horizontal planes at $z = 0.25$, 0.5 and 0.75, where each arrow's colour denotes the value of w as shown in a colour bar on the right hand. We can confirm that instantaneous flow structure is the same as the S5 at anytime.

Figures 10 and 11 show time histories of $u_{(0.75H,\,0.75H,\,0.75H)}$, and their corresponding spectra, for $Ra = 2.5\times10^5$ and $Pr = 7.1$ with decreasing Ra, and for $Ra = 3.3\times10^5$ and $Pr = 7.1$ with increasing Ra, respectively. Both the figures represent the Chaotic.

At first, we see Fig. 10. Although figure (a) shows poor periodicity, we can observe a clear spectrum peak in figure (b). Next, we see Fig. 11. Figure (a) shows not an exact periodicity, but a close periodicity. In fact, we can observe a sharp spectrum peak in figure (b). As a result, flow in the Chaotic always fluctuates with one dominant frequency, in spite of the degree of less periodicity.

Figure 12 summarises such a dominant frequency. Namely, the figure shows a non-dimensional frequency Ω of oscillatory convection in the $S5_p$ and the Chaotic, plotted against Ra. We can see that $\Omega \approx 300$ at $Ra = 2.28\times10^5$ — 2.45×10^5, and that $\Omega \approx 200$ at $Ra = 2.50\times10^5$ — 3.50×10^5. This suggests that the $S5_p$ at $Ra = 2.28\times10^5$ — 2.36×10^5 is not the same as that at $Ra = 2.62\times10^5$ — 3.10×10^5, from a viewpoint of oscillatory-convection frequency. Accordingly, the Chaotic at $Ra = 2.36\times10^5$ — 2.60×10^5 shows a transition feature between the two different $S5_P$, and is considered to be different from the Chaotic at $Ra = 3.10\times10^5$ — 3.50×10^5.

Kinetic Energy and Nusselt Number

Figure 13 shows a time-mean spatially-averaged kinetic energy $\overline{K}_{\mathrm{mean}}$ plotted against Ra, for $Pr = 7.1$. And, Fig. 14 shows a time-mean inflow-average Nusselt number $Nu_{\text{inflow-ave, mean}}$ plotted against Ra, for $Pr = 7.1$. In both Figs. 13 and 14, figures (a) and (b) represent the results for decreasing Ra and increasing Ra, respectively.

The increasing rate of the $\overline{K}_{\mathrm{mean}}$ with increasing Ra shows a different manner from that of $Nu_{\text{inflow-ave, mean}}$, that is, the former is progressive and the latter is asymptotic as Ra increases.

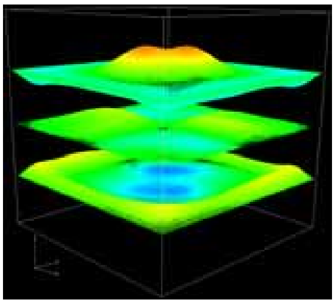
(a) At t = 5.016: point A in Fig. 8

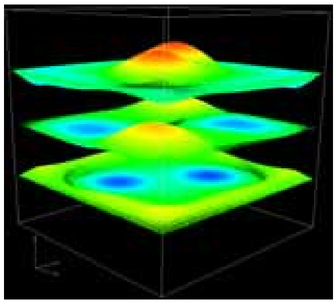
(b) At t = 5.022: point B in Fig. 8

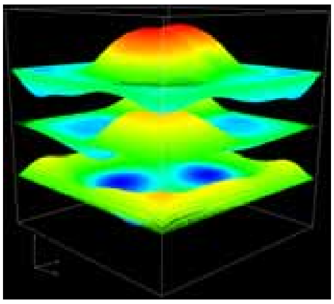
(c) At t = 5.026: point C in Fig. 8

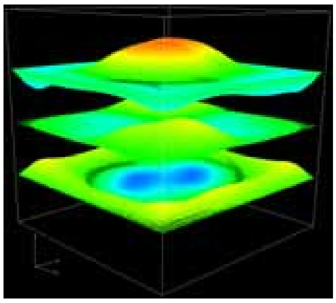
(d) At t = 5.030: point D in Fig. 8

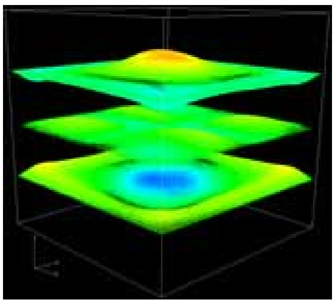
(e) At t = 5.034: point E in Fig. 8

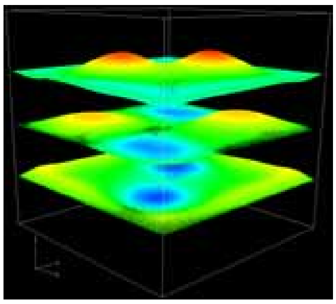
(f) At t = 5.037: point F in Fig. 8

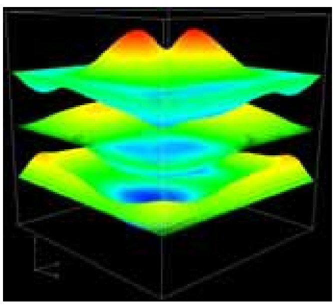
(g) At t = 5.041: point G in Fig. 8

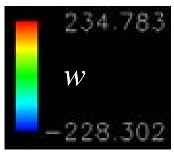

Fig. 9 Flow structure $S5_p$, for *Ra* = 2.65×10^5 and *Pr* = 7.1with increasing *Ra* (Perspective views of velocity vectors on the three horizontal plane at *z* = 0.25, 0.5 and 0.75). Each arrow's colour denotes the value of *w* as shown in a colour bar.

In Figs. 13(b) and 14(b), we can confirm hysterisis effects on $\overline{K}_{\mathrm{mean}}$ and $Nu_{\text{inflow-ave, mean}}$ at Ra = 2.28×10^5 — 2.62×10^5, respectively. This suggests that the values of $\overline{K}_{\mathrm{mean}}$ and $Nu_{\text{inflow-ave, mean}}$ in the oscillatory convection of the S5$_{\mathrm{p}}$ tend to be smaller than those in the steady convection of the S6, respectively. Then, there exist small jumps/drops of $\overline{K}_{\mathrm{mean}}$ and $Nu_{\text{inflow-ave, mean}}$ at $Ra = Ra_{c2}$.

CONCLUSIONS

We have specified the second and third critical Rayleigh numbers — Ra_{c2} and Ra_{c3}, indicating the transition to oscillatory flow and turbulent flow, respectively. We have found that Ra_{c2} and Ra_{c3} are roughly 2.6×10^5 and 3.1×10^5, respectively. And, we have observed a histerisis effect upon the value of Ra_{c2} with chaotic behaviour at $Ra \approx Ra_{c2}$, and revealed flow structures such as S2, S1, S5, S6 and S5$_{\mathrm{p}}$. In addition, we investigate the relationship between Ra and the oscillatory-convection frequency. The S5$_{\mathrm{p}}$ at Ra = 2.28×10^5 — 2.36×10^5 is not the same as that at Ra = 2.62×10^5 — 3.10×10^5, from a viewpoint of oscillatory frequency. Accordingly, the Chaotic at Ra = 2.36×10^5 — 2.60×10^5 shows a transition feature between the two different S5$_{\mathrm{P}}$. The increasing rate of the $\overline{K}_{\mathrm{mean}}$ with increasing Ra shows a different manner from that of $Nu_{\text{inflow-ave, mean}}$, that is, the former is progressive and the latter is asymptotic as Ra increases. Both the values of $\overline{K}_{\mathrm{mean}}$ and $Nu_{\text{inflow-ave, mean}}$ in oscillatory flow tend to be smaller than those in steady flow, respectively. Then, there exist small jumps/drops of $\overline{K}_{\mathrm{mean}}$ and $Nu_{\text{inflow-ave, mean}}$ at $Ra = Ra_{c2}$.

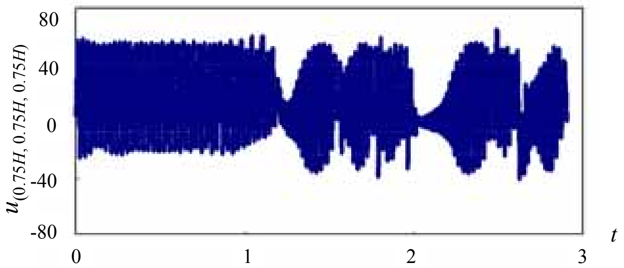

(a) Time history

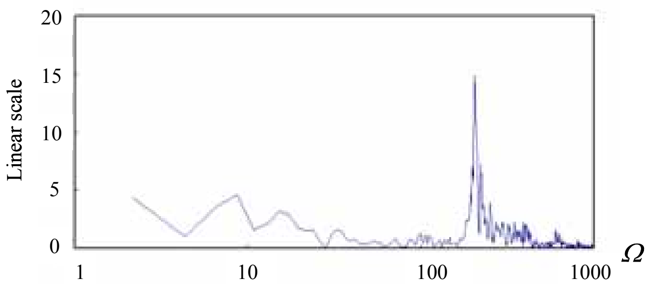

(b) Spectrum

Fig. 10 Time history of $u_{(0.75H,\,0.75H,\,0.75H)}$ and its spectrum for Ra = 2.5 × 10^5 and Pr = 7.1 with decreasing Ra (Chaotic).

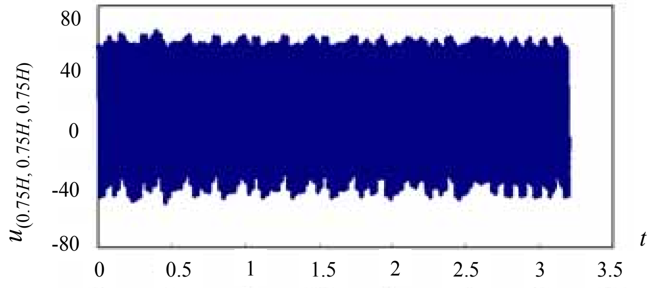

(a) Time history

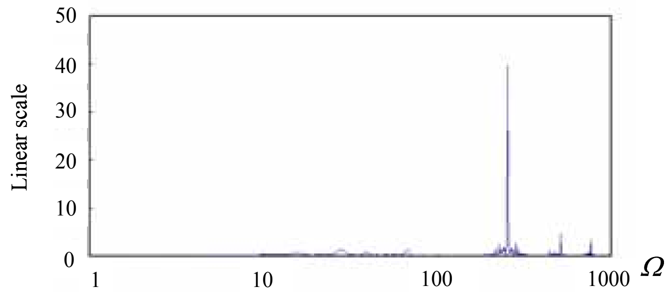

(b) Spectrum

Fig. 11 Time history of $u_{(0.75H,\,0.75H,\,0.75H)}$ and its spectrum for Ra = 3.3×10^5 and Pr = 7.1 with increasing Ra (Chaotic).

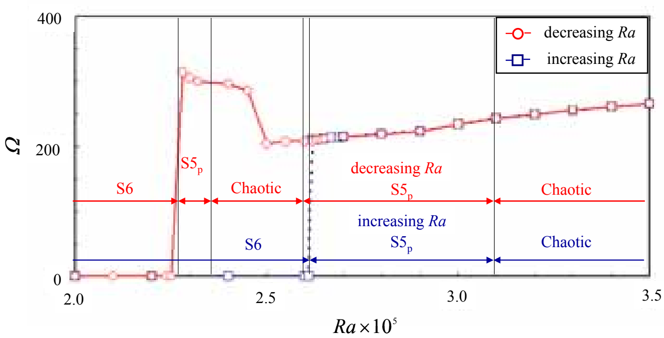

Fig. 12 Non-dimensional frequency Ω of oscillatory convection in S5$_{\mathrm{p}}$ and Chaotic for Ra = 2.0 × 10^5 – 3.5 × 10^5 and Pr = 7.1.

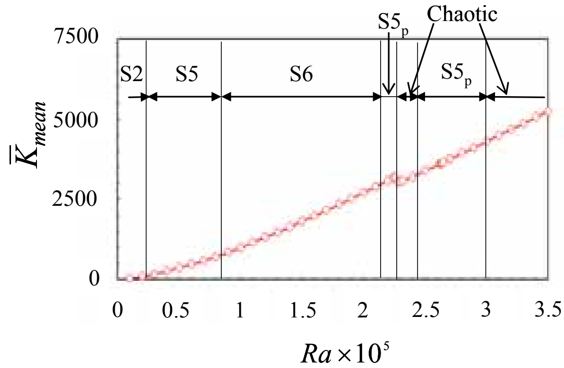

(a) decreasing *Ra*

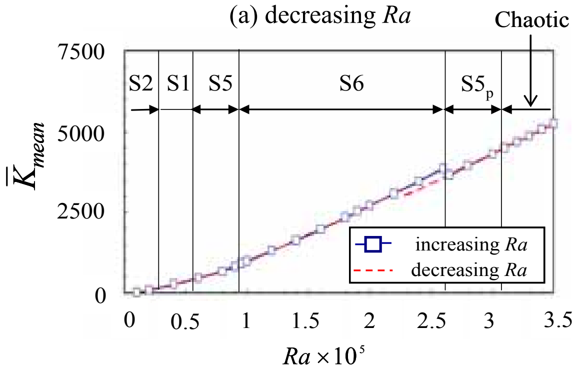

(b) increasing *Ra*

Fig. 13 Time-mean spatially-averaged kinetic energy K_{mean} against *Ra* for *Pr* = 7.1.

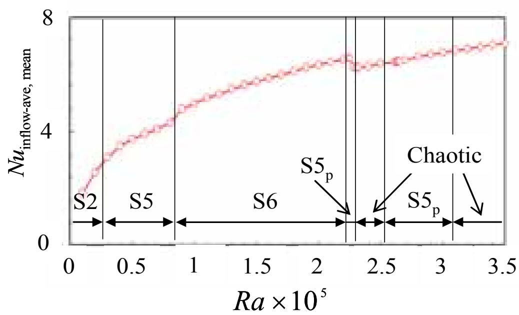

(a) decreasing *Ra*

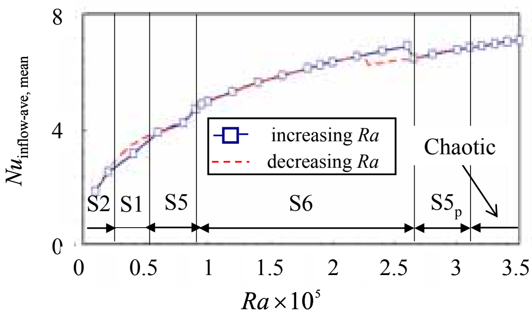

(b) increasing *Ra*

Fig. 14 Time-mean inflow-averaged Nusselt number $Nu_{inflow\text{-}ave,\ mean}$ against *Ra* for *Pr* = 7.1.

NOMENCLATURE

$\boldsymbol{e}_z$	unit vector in the *z* direction	
g^*	gravitational acceleration	[m/s^2]
H^*	height of a cavity	[m]
K	kinetic energy (non-dimensional)	
M	mesh size	
Nu	Nusselt number	
p	pressure (non-dimensional)	
Pr	Prandtl number	
Ra	Rayleigh number	
T	temperature (non-dimensional)	
t	time (non-dimensional)	
Δt	time step (non-dimensional)	
u, v	horizontal components of velocity (non-dimensional)	
$\boldsymbol{u}$	velocity vector (non-dimensional)	
V	volume of a cavity (non-dimensional)	
w	vertical component of velocity (non-dimensional)	
x, y	coordinates in the horizontal directions (non-dimensional)	
z	coordinate in the vertical direction (non-dimensional)	

Greek Letters

α^*	thermal diffusivity	[m^2/s]
β^*	thermal expansion coefficient	[1/K]
φ	irreversibility distribution ratio	
υ^*	kinetic viscosity	[m^2/s]
ρ^*	density	[kg/m^3]
Ω	(angular) frequency (non-dimensional)	

Superscripts

*	dimensional
$\bar{\ }$	spatially-averaged

Subscripts

c	on cold wall
h	on hot wall
inflow-ave	inflow-average
local	local
mean	time-mean

REFERENCES

1. R. J. A. Janssen, R. A. W. M. Henkes & C. J. Hoogendoorn, Transition to time-periodicity of a natural-convection flow in a 3D differentially heated cavity, *Int. J. Heat Mass Transf.*, 36 (1993) 2927-2940.
2. J. Pallares, I. Cuesta, F. X. Grau & F. Giralt, Natural convection in a cubical cavity heated from below at low Rayleigh numbers, *Int. J. Heat Mass Transf.*, 39 (1996) 3233-3247.
3. J. Pallares, F. X. Grau & F. Giralt, Flow transitions in laminar Rayleigh-Bénard convection in a cubic cavity at moderate Rayleigh numbers, *Int. J. Heat Mass Transf.*, 42 (1999) 753-769.

4. J. Pallares, M. P. Arroyo, F. X. Grau & F. Giralt, Experimental laminar Rayleigh-Bénard convection in a cubical cavity at moderate Rayleigh and Prandtl number, *Experiments in Fluids*, 31 (2001) 208-218.
5. J. Pallares, I. Cuesta & F. X. Grau, Laminar and turbulent Rayleigh-Bénard convection in a perfectly conducting cubical cavity, *Int. J. Heat Fluid Flow*, 23 (2002) 346-358.
6. H. Hirano, H. Ozoe & N. Okamoto, Experimental study of natural convection heat transfer of air in a cube below atmospheric pressure, *Int. J. Heat Mass Transf.*, 46 (2003) 4483-4488.
7. E. Brown, A. Nikolaenko, D. Funfschilling & G. Ahlers, Heat transport in turbulent Rayleigh-Bénard convection: Effect of finite top- and bottom-plate conductivities, *Physics of Fluids*, 17 (2005) 1-10.
8. D. W. Crunkleton, R. Narayanan & T. J. Anderson, Numerical simulation of periodic flow oscillations in low Prandtl number fluids, *Int. J. Heat Mass Transf.*, 49 (2006) 427-438.
9. K. Hirata, R. Hakui, K. Ishihara, H. Tanigawa & J. Funaki, On frequency response of fluid in a cubic cavity heated below, *Trans. JSME, Series B,* 72 (2006) 279-284 (in Japanese).
10. B. A. V. Bennett & J. Hsueh, Natural convection in a cubic cavity: Implicit numerical solution of two benchmark problems, *Numerical Heat Transfer, Part A: Applications*, 50 (2006) 99-123
11. L. Valencia, J. Pallares, I. Cuesta & F. X. Grau, Turbulent Rayleigh-Bénard convection of water in cubical cavities: A numerical and experimental study, *Int. J. Heat Mass Transf.*, 50 (2007) 3203-3215.